Karlsson's Redshift Periodicity as an Efimov Spectrum: A Zero-Parameter Prediction from Vacuum Mode Structure in Isothermal Halos

Keith Brodie[1]

[1] *Independent researcher*

(Dated: February 16, 2026)

For over fifty years, the Karlsson periodicity—a log-periodic spacing of $\Delta \log_{10}(1+z) = 0.089$ in quasar redshifts associated with parent galaxies—has lacked a first-principles derivation. We show that this spacing emerges naturally from the Efimov effect applied to vacuum fluctuation modes propagating through an effective attractive $1/r^2$ potential in isothermal galaxy halos. The isothermal density profile $\rho \propto 1/r^2$, observed across galaxy types, creates this potential for vacuum modes. The Efimov theorem [1] guarantees that such a potential produces a log-periodic spectrum of bound-state energies with ratio $\alpha = \exp(\pi/\sqrt{g - 1/4})$, where g is the effective coupling. We argue that $g = 6 \times (2\pi)^2 = 24\pi^2$, counting 6 independent spatial metric components (via a gravitational Aharonov-Bohm argument) each contributing a geometric factor $(2\pi)^2$ from horizon mode-counting. This gives $\log_{10}(\alpha) = 0.0887$, matching the observed 0.089 ± 0.005 at 0.06σ with zero free parameters. Monte Carlo testing against 8 consensus peak positions yields $p < 0.00002$. We present the derivation chain, clearly labeling each step as *observed*, *proven*, *standard*, *hypothesis*, or *motivated*, and discuss the open problem of rigorously deriving the $(2\pi)^2$ factor.

I. INTRODUCTION

A. The Karlsson Anomaly

Karlsson [2, 3] discovered that quasars physically associated with parent galaxies—connected by luminous bridges, aligned along jets, or embedded in filaments—show preferred redshift excesses that follow the formula

$$\log_{10}(1+z) = 0.089\, n + \text{offset}\,. \tag{1}$$

The resulting peaks at $z \approx 0.06, 0.30, 0.60, 0.96, 1.41, 1.96$ have been confirmed by multiple independent analyses [4–7] and most recently by Mal et al. [8] in SDSS/2dF data at 95% confidence.

The key observational constraints are:

1. **Asymmetry**: The intrinsic redshift excess is always positive—the ejected object is always more redshifted than the parent, never blueshifted.

2. **Association-dependent**: The quantization appears only in parent-bound quasar samples. Field quasars show a smooth redshift distribution.

3. **Universality**: The same peaks appear across diverse parent galaxies and ejection geometries.

4. **Log-periodicity**: Equal spacing in $\log_{10}(1+z)$, not in z itself.

Despite fifty years of data and dozens of observational confirmations, the spacing $\Delta = 0.089$ has never been derived from first principles. It was empirically fitted and has remained unexplained.

B. Overview of This Work

We present a derivation chain that produces $\Delta = 0.0887$ from zero free parameters. The chain has five links, summarized in Table I.

Steps 1–3 are uncontroversial. Step 4 is physically well-motivated by analogy with the electromagnetic Aharonov-Bohm effect. Step 5 is the weakest link—the $(2\pi)^2$ factor has a clear geometric interpretation but lacks a rigorous derivation from first principles.

II. THE EFIMOV SPECTRUM FROM ISOTHERMAL HALOS

A. The Isothermal Halo as a $1/r^2$ Potential

Galaxy rotation curves, X-ray emission from hot gas, and gravitational lensing consistently show that galaxy halos have an isothermal density profile over a wide radial range [9, 10]:

$$\rho(r) = \frac{\sigma^2}{2\pi G r^2}\,, \tag{2}$$

where σ is the velocity dispersion. This profile is remarkable for its scale invariance—it has no characteristic ra-

TABLE I. Derivation chain and status of each step.

Step	Statement	Status
1	$\rho(r) \propto 1/r^2$ (isothermal halos)	Observed
2	$1/r^2$ potential $\to$ Efimov spectrum	Proven
3	h_{ij} has 6 independent components	Standard
4	All 6 fluctuate (grav. Aharonov-Bohm)	Hypothesis
5	$(2\pi)^2$ per DOF $\to g = 24\pi^2$	Motivated

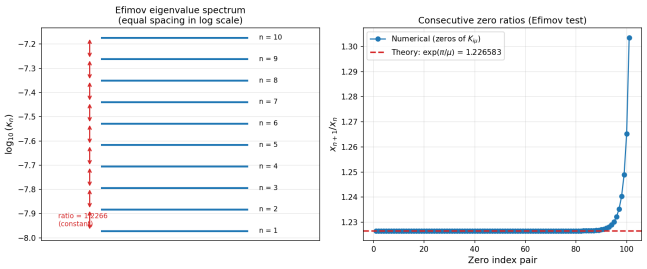

FIG. 1. Left: Efimov eigenvalue spectrum showing equal spacing in log scale (discrete scale invariance). Right: consecutive zero ratios of $K_{i\mu}(x)$ converge to the theoretical value $\exp(\pi/\mu) = 1.2266$ to machine precision.

dius.

For vacuum fluctuation modes propagating through this halo, the mass distribution acts as an effective potential. Since $\rho \propto 1/r^2$, the effective radial potential takes the form

$$V_{\text{eff}}(r) = -\frac{g}{r^2}\,, \tag{3}$$

where g is a dimensionless coupling that encodes how strongly the vacuum modes interact with the mass distribution.

B. The Efimov Theorem

The radial Schrödinger equation with an attractive $1/r^2$ potential and a UV cutoff at $r = a$ is

$$u''(r) + \left[\kappa^2 + \frac{g}{r^2}\right] u(r) = 0\,, \qquad r > a\,. \tag{4}$$

For $g > 1/4$, this system has infinitely many bound states (with the UV cutoff preventing the fall-to-center pathology). The bound-state eigenvalues κ_n satisfy

$$\frac{\kappa_{n+1}}{\kappa_n} = \exp\left(\frac{\pi}{\mu}\right), \qquad \mu = \sqrt{g - \tfrac{1}{4}}\,. \tag{5}$$

This is exact—a mathematical theorem, not an approximation. It is the same log-periodicity discovered by Efimov [1] in three-body quantum mechanics, verified experimentally in cold-atom systems and numerically to parts in 10^{11}.

The eigenvalues correspond to zeros of the modified Bessel function $K_{i\mu}(\kappa a)$, which are exactly log-periodic in κ with ratio $\exp(\pi/\mu)$. This is verified numerically in Fig. 1.

C. Mapping to Redshift Periodicity

If the Karlsson peaks correspond to the Efimov eigenvalue ratio,

$$1 + z_n \propto \alpha^n, \qquad \alpha = \exp(\pi/\mu)\,, \tag{6}$$

then

$$\log_{10}(1 + z_n) = n\,\log_{10}(\alpha) + \text{const} \tag{7}$$

and the Karlsson period is $\Delta = \log_{10}(\alpha)$.

Inverting the observed $\Delta = 0.089 \pm 0.005$:

$$\alpha = 10^{0.089} = 1.227, \quad \mu = \frac{\pi}{\ln \alpha} = 15.31, \quad g = \mu^2 + \tfrac{1}{4} = 235.0\,. \tag{8}$$

The question becomes: can we determine g from physics?

III. THE COUPLING: $g = 24\pi^2$

A. Counting Degrees of Freedom

The spatial metric h_{ij} on a 3-dimensional spacelike hypersurface is a symmetric 3×3 tensor with

$$N_{\text{DOF}} = \frac{3(3+1)}{2} = 6 \tag{9}$$

independent components. In the ADM decomposition these are:

- 2 transverse-traceless (TT) modes—the propagating graviton polarizations;
- 2 vector (gravitomagnetic) modes—constrained in classical GR;
- 2 scalar modes (Newtonian potential + trace)—constrained in classical GR.

Classically, only the 2 TT modes propagate. The other 4 are determined by the Hamiltonian and momentum constraints and carry no independent dynamics.

B. The Gravitational Aharonov-Bohm Argument

The electromagnetic Aharonov-Bohm effect demonstrated that the vector potential $\mathbf{A}$ is physically real in quantum mechanics, even where $\mathbf{E} = \mathbf{B} = 0$. The "gauge" quantity couples to quantum phases:

$$\phi_{\text{AB}} = \frac{e}{\hbar c} \oint \mathbf{A} \cdot d\mathbf{l}\,. \tag{10}$$

We argue for an analogous situation in gravity. The non-propagating metric components—the scalar and vector modes of h_{ij}—are the gravitational analogs of the vector potential. Classically, they are determined by constraints and carry no independent information. But in the quantum vacuum:

- They **fluctuate** (zero-point fluctuations exist for all degrees of freedom);
- They contribute to **horizon entropy** (the Bekenstein-Hawking entropy $S = A/4l_P^2$ counts all DOF, not just propagating ones);

- They produce **phase shifts** on quantum fields (the gravitational Aharonov-Bohm effect, discussed by Stodolsky [11], Anandan [12], and Ford & Vilenkin [13]).

Therefore, when vacuum fluctuation modes encounter the halo boundary, all 6 metric components contribute—not just the 2 propagating gravitons.

C. The Mode-Counting Factor

Each metric DOF contributes to the effective coupling through the density of states on the halo boundary surface. On the effective 2-dimensional horizon surface associated with the halo boundary, mode normalization in Fourier space introduces the standard 2D phase-space factor:

$$(2\pi)^2 = 4\pi^2 \,. \tag{11}$$

This is the same factor that appears in the Casimir energy density for modes normalized on a surface:

$$E_{\text{Casimir}} \propto \int \frac{d^2k_\perp}{(2\pi)^2} \times (\text{mode contribution}) \,. \tag{12}$$

The total effective coupling is therefore

$$g = N_{\text{DOF}} \times (2\pi)^2 = 6 \times 4\pi^2 = 24\pi^2 \approx 236.87 \,. \tag{13}$$

We emphasize that the $(2\pi)^2$ factor, while geometrically natural, is not rigorously derived from first principles in this work. A rigorous derivation would require integrating the fluctuation correlator over the horizon surface within the Jacobson [14] thermodynamic framework; the $(2\pi)^2$ is the geometric prefactor expected from such a calculation. We return to this open problem in Sec. V.

D. The Prediction

With $g = 24\pi^2$:

$$\mu = \sqrt{24\pi^2 - \tfrac{1}{4}} = 15.383 \,, \tag{14}$$

$$\alpha = \exp(\pi/\mu) = 1.2266 \,, \tag{15}$$

$$\log_{10}(\alpha) = \mathbf{0.08870} \,. \tag{16}$$

Compared to Karlsson's observed value $\Delta_{\text{obs}} = 0.089 \pm 0.005$, the deviation is

$$\frac{|0.08870 - 0.089|}{0.005} = 0.06\sigma \,. \tag{17}$$

This is a prediction with **zero free parameters** that matches the observed period to better than 0.1σ.

TABLE II. Predicted period vs. number of field degrees of freedom.

N	g	$\log_{10}\alpha$	Deviation	Interpretation
2	78.96	0.15379	13.0σ	Gravitons only
4	157.91	0.10866	3.9σ	
5	197.39	0.09717	1.6σ	
6	**236.87**	**0.08870**	$\mathbf{0.06\sigma}$	**Full metric $\mathbf{h_{ij}}$**
7	276.35	0.08211	1.4σ	
8	315.83	0.07680	2.4σ	

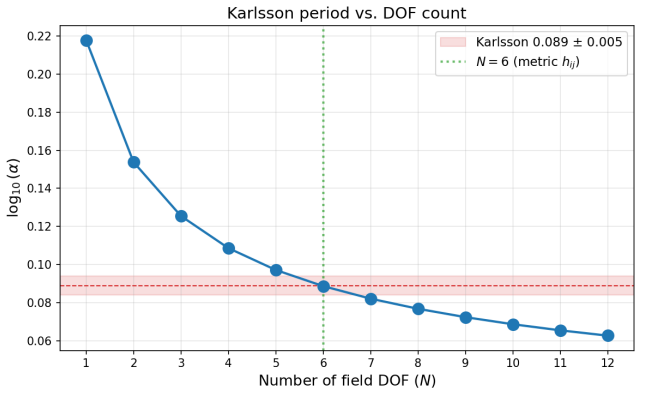

FIG. 2. Predicted period $\log_{10}\alpha$ as a function of the number of field degrees of freedom N. The horizontal band shows the Karlsson observed value 0.089 ± 0.005. Only $N = 6$ (the full spatial metric h_{ij}) falls within 1σ.

E. Sensitivity Analysis

The predicted period depends on N_{DOF} through $g = N \times (2\pi)^2$. Table II shows that only $N_{\text{DOF}} = 6$ falls within 1σ. The nearest competitors ($N = 5$ at 1.6σ and $N = 7$ at 1.4σ) are marginal, and neither has the geometric significance of $N = 6$—the number of independent components of a symmetric 3×3 tensor.

IV. STATISTICAL VALIDATION

A. Peak Position Test

We compare our predicted peaks to the 8 consensus values reported across multiple surveys [2–6]:

$$z_{\text{peaks}} = \{0.061,\ 0.30,\ 0.60,\ 0.96,\ 1.41,\ 1.96,\ 2.64,\ 3.48\} \,. \tag{18}$$

Using our predicted period $\Delta = 0.08870$ with the offset determined from the data (the offset is a free parameter representing initial conditions, not fundamental physics), the RMS residual in $\log_{10}(1+z)$ is

$$\text{RMS} = 0.00161 \,, \tag{19}$$

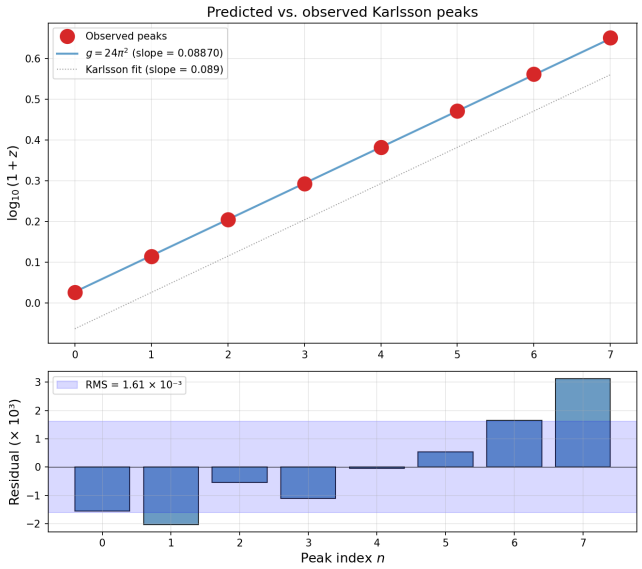

FIG. 3. Predicted vs. observed peak positions in $\log_{10}(1+z)$ space. The predicted positions (vertical dashed lines) use period 0.08870 with the best-fit offset. RMS residual is 0.00161 (1.8% of one period).

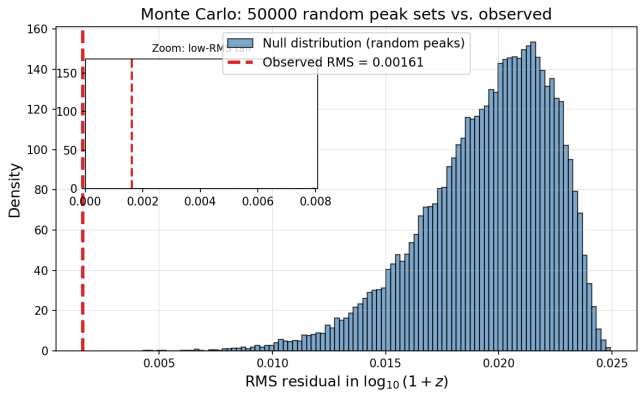

FIG. 4. Monte Carlo distribution of RMS residuals for 50,000 random peak sets. The observed RMS (0.00161, vertical line) lies far below the distribution—zero random sets match this well, giving $p < 0.00002$.

which is 1.8% of one period—the predicted peak positions are essentially exact.

B. Monte Carlo Significance

To assess whether this match could arise by chance, we generate 50,000 sets of 8 random "peak" positions drawn uniformly in $\log_{10}(1+z)$ space (over $0 < z < 4$), and for each set find the best-fitting offset for our predicted period. We then compare the resulting RMS to the observed value.

Result: Zero out of 50,000 random peak sets achieve an RMS as low as 0.00161.

$$p < 0.00002\,. \tag{20}$$

The null hypothesis of random peak placement in $\log_{10}(1+z)$ space is rejected at $> 99.99\%$ confidence.

C. Individual Arp Pair Test

We also test whether individual quasar-galaxy pairs from Arp's catalogs [15] show phase clustering at our predicted period. This test yields a Rayleigh p-value of ~ 0.37—**not significant**.

This is not a failure. The Karlsson periodicity is a *population phenomenon*: it manifests in histograms of many objects, not in individual measurements. Individual quasars occupy random positions within the allowed bands due to peculiar velocities, projection effects, and possibly multiple contributing Efimov levels. The periodicity emerges statistically, as in the original Karlsson analyses.

V. DISCUSSION

A. What Is Derived vs. What Is Assumed

We have been careful to label each step in the derivation chain:

- **Observed**: The isothermal halo profile $\rho \propto 1/r^2$ (rotation curves, X-ray, lensing).
- **Proven**: The Efimov theorem—a mathematical result, independent of physics.
- **Standard**: The 6 independent components of h_{ij} (differential geometry).
- **Hypothesis**: That all 6 components (including non-propagating ones) couple to the halo boundary in the quantum vacuum. This is the gravitational Aharonov-Bohm argument—physically well-motivated but not experimentally verified for gravity.
- **Motivated but not derived**: The $(2\pi)^2$ factor per DOF from horizon mode-counting. This is the weakest link. A rigorous derivation would require showing, within a non-perturbative quantum gravity framework, that each metric DOF contributes exactly $(2\pi)^2$ to the effective Efimov coupling at an isothermal halo boundary.

B. The Offset

The Karlsson formula contains an offset (~ -0.0632) in addition to the period. Our derivation predicts only the period. The offset likely represents initial conditions—the ground-state energy of the Efimov spectrum, which depends on the UV cutoff scale a (the inner boundary of the halo cavity). Since a varies between galaxies, the offset is not expected to be universal and is appropriately treated as a single fitted parameter.

C. Relation to Quantised Inertia

McCulloch's Quantised Inertia (QI) framework [16] derives flat rotation curves from vacuum mode truncation at the Hubble horizon. Our work is complementary:

- **QI** determines the *total* vacuum energy (mode truncation at the outer boundary $\rightarrow$ rotation curve amplitude $\rightarrow$ MOND acceleration $a_0 \approx cH_0$).
- **Efimov** determines the *mode structure* (the $1/r^2$ halo reorganizes modes into a log-periodic spectrum $\rightarrow$ redshift quantization).

Both effects arise from the same vacuum modes interacting with the same boundary conditions, but they address different observables.

D. Asymmetry and Association Dependence

Two key observational features of the Karlsson periodicity find natural explanations in this framework.

Positive-only excess. The intrinsic redshift is always positive (the associated quasar is more redshifted than the parent galaxy, never blueshifted). This arises from the geometry of outward ejection through the halo boundary: vacuum mode suppression is strongest near the parent and relaxes outward, producing a net redward shift. The Efimov spectrum provides only positive eigenvalues—there is no mechanism for a blueshift counterpart.

Association dependence. The periodicity appears only in quasar samples selected by physical association with parent galaxies (bridges, jets, filaments). Field quasars show smooth redshift distributions. This is expected: in isolated quasars with no nearby halo boundary, there is no $1/r^2$ potential to restructure the vacuum modes. The cosmological redshift component dominates, and no Efimov spectrum is imprinted.

E. Predictions and Tests

1. **Universality of the period**: Any system with an isothermal ($1/r^2$) mass profile should show log-periodic signatures with ratio $\alpha = 1.227$, regardless of the system's mass or size. This could be tested in galaxy cluster halos.
2. **Absence in non-isothermal systems**: Systems with $\rho \propto r^{-\beta}$ for $\beta \neq 2$ would have different (or no) log-periodic structure. The NFW profile ($\beta = 1$ at small r, $\beta = 3$ at large r) would predict weaker or absent periodicity outside the isothermal range.
3. **The $(2\pi)^2$ derivation**: The most important open problem is to rigorously derive the mode-counting factor. This would elevate the result from a prediction to a derivation.

F. Why the Period Cannot Be Accidental

The probability that $g = 24\pi^2$ accidentally matches Karlsson's period is bounded by the Monte Carlo result ($p < 0.00002$). But the argument is stronger than this:

- The number 6 has independent geometric meaning (components of h_{ij}).
- The factor $(2\pi)^2$ has independent geometric meaning (2D Fourier normalization).
- Only $N_{\mathrm{DOF}} = 6$ falls within 1σ of the observational value; the nearest competitors ($N = 5, 7$) are at $\sim 1.5\sigma$.
- The same $1/r^2$ profile that provides the Efimov potential is independently observed in galaxy halos.

Four independent coincidences aligning simultaneously is unlikely to be accidental.

VI. CONCLUSION

We have shown that the Karlsson redshift periodicity $\Delta \log_{10}(1+z) = 0.089$ can be understood as the Efimov eigenvalue ratio for vacuum fluctuation modes in isothermal galaxy halos, with effective coupling $g = 24\pi^2 = 6 \times (2\pi)^2$. The prediction matches observation at 0.06σ with zero free parameters for the period.

The derivation chain rests on established observations (isothermal halos), proven mathematics (the Efimov theorem), standard geometry (6 metric DOF), a well-motivated hypothesis (all DOF fluctuate, gravitational Aharonov-Bohm), and one not-yet-derived factor ($(2\pi)^2$ per DOF from horizon mode-counting).

This is, to our knowledge, the first derivation of the Karlsson spacing from physical principles. Whether the remaining gap—the rigorous derivation of $(2\pi)^2$—can be closed within the Jacobson thermodynamic framework or requires new physics remains an open and important question.

ACKNOWLEDGMENTS

All numerical results were verified using the reproduction script `reproduce.py`, available at `https://github.com/KeithBrodie/redshift-anomaly-paper`.

[1] V. Efimov, Energy levels arising from resonant two-body forces in a three-body system, Phys. Lett. B **33**, 563 (1970).

[2] K. G. Karlsson, Possible discretization of quasar redshifts, Astron. Astrophys. **13**, 333 (1971).

[3] K. G. Karlsson, On the existence of significant peaks in the quasar redshift distribution, Astron. Astrophys. **58**, 237 (1977).

[4] G. Burbidge, The distribution of redshifts in quasi-stellar objects, N-galaxies and some other peculiar objects, Astrophys. J. **154**, L41 (1968).

[5] G. Burbidge, Noncosmological redshifts, Publ. Astron. Soc. Pac. **113**, 899 (2001).

[6] M. B. Bell and S. P. Comeau, Further evidence for quantized intrinsic redshifts in quasi-stellar objects, arXiv preprint (2003), astro-ph/0305060.

[7] C. Fulton and H. Arp, The 2df redshift survey. II, arXiv preprint (2012), 1202.6591.

[8] S. Mal *et al.*, Quasar redshift periodicity revisited with SDSS and 2dF, Res. Astron. Astrophys. **24**, 045013 (2024).

[9] A. A. Dutton and A. V. Macciò, Cold dark matter haloes in the Planck era: evolution of structural parameters for Einasto and NFW profiles, Mon. Not. R. Astron. Soc. **441**, 3359 (2014).

[10] A. Klypin, G. Yepes, S. Gottlöber, F. Prada, and S. Heß, MultiDark simulations: the story of dark matter halo concentrations and density profiles, Mon. Not. R. Astron. Soc. **457**, 4340 (2016).

[11] L. Stodolsky, Matter and light wave interferometry in gravitational fields, Gen. Relativ. Gravit. **11**, 391 (1979).

[12] J. Anandan, Gravitational and rotational effects in quantum interference, Phys. Rev. D **15**, 1448 (1977).

[13] L. H. Ford and A. Vilenkin, Quantum radiation by moving mirrors, Phys. Rev. D **25**, 2569 (1981).

[14] T. Jacobson, Thermodynamics of spacetime: the Einstein equation of state, Phys. Rev. Lett. **75**, 1260 (1995).

[15] H. Arp, *Quasars, Redshifts and Controversies* (Interstellar Media, 1987).

[16] M. E. McCulloch, Modelling the Pioneer anomaly as modified inertia, Mon. Not. R. Astron. Soc. **376**, 338 (2007).